Er-Doped AlGaAs Native Oxides: Photoluminescence Characterization and Process Optimization

Leigang Kou, Douglas C. Hall, *Member, IEEE*, Christof Strohhöfer, Albert Polman, Tong Zhang, Robert M. Kolbas, *Fellow, IEEE*, Richard D. Heller, Jr., and Russell D. Dupuis, *Fellow, IEEE*

***Abstract*—We present 300 K photoluminescence (PL) characterization data for wet thermal native oxides of $Al_{0.58}Ga_{0.42}As$ films grown by metal organic chemical vapor deposition and doped with Er via multiple high-energy ion implants (for 0.0675, 0.135, and 0.27 atomic percent (at.%) peak Er concentrations), and $Al_{.5}Ga_{.5}As$ and $Al_{0.8}In_{0.2}As$ films doped with Er (0.03–0.26 at.%) during molecular beam epitaxy crystal growth. Broad spectra with a ~50-nm full-width at half-maximum and a PL peak at 1.534 μm are observed, characteristic of Al_2O_3:Er films. The dependencies of PL intensity, spectra, and lifetime on annealing temperature (675 °C–900 °C), time (2–60 min) and As overpressure (0–0.82 atm) are studied to optimize the annealing process, with As considered as a possible quenching mechanism. Wet and dry-oxidized films are compared to explore the role of hydroxyl (OH) groups identified by Fourier transform infrared (FTIR) spectroscopy. FTIR experiments employing heavy water (D_2O) suggest that OH groups in wet oxidized AlGaAs come mainly from post-oxidation adsorption of atmospheric moisture. AlGaAs:Er films wet oxidized with 0.1% O_2 added to the N_2 carrier gas show a fourfold PL intensity increase, doubled PL lifetime to $\tau \sim 5.0$ ms (0.27 at.% implanted sample), and the lowest degree of concentration quenching.**

***Index Terms*—Aluminum alloys, erbium, integrated optoelectronics, materials processing, optical amplifiers, oxidation, photoluminescence, semiconductor films.**

I. Introduction

MOTIVATED by the widespread application of the rare earth element Er for signal amplification near $\lambda = 1.54$ μm in optical fiber telecommunications systems [1], [2], the rare-earth-doping of semiconductors has been extensively explored to increase the potential integration of optical and electronic components [3], [4]. In an earlier work [5], we demonstrated a new approach for incorporating Er into the AlGaAs–GaAs compound semiconductor system by converting Er-doped AlGaAs to its native oxide by wet-thermal oxidation [6], [7]. Strong room temperature (300 K), continuous wave Er^{3+} photoluminescence (PL) with a lifetime as long as 7 ms was observed from oxidized AlGaAs with shallow doping via an 80-keV Er^{2+} ion implantation prior to oxidation [5]. These native oxides, close in nature to Al_2O_3 [8], are naturally more suitable hosts for trivalently ionized Er^{3+} atoms than the unoxidized semiconductors. This is due to the similarity in valency and lattice constants between Al_2O_3 and Er_2O_3, which leads to greater solubility and optical activation of the Er. There has also been considerable recent interest in Er-doped thin-film materials for the development of planar waveguide amplifiers [9]–[23]. Among these, Al_2O_3:Er thin films are the most widely explored because of the possibility for incorporating high concentrations of Er, for the large inhomogeneous broadening of Er, which yields a large (~55 nm) spectral bandwidth well suited to wavelength-division-multiplexing (WDM) applications, and for the ability to realize low-loss waveguides. A net optical gain of 2.3 dB has been realized for a 4-cm-long Al_2O_3:Er waveguide with 9 mW of 1.48-μm pump power [12], and recent simulations predict greater gain with the use of Er^{3+}–Yb^{3+} codoping [22], [23]. One motivation for exploring Er-doped AlGaAs films is the potential for realizing a 1.55-μm planar oxide waveguide amplifier monolithically-integrated with other electronic or optoelectronic components, such as a 980-nm InGaAs quantum-well (QW) pump laser, or 1.55-μm GaInNAs QW signal lasers [24] or detectors. We have previously demonstrated the possibility for realizing an oxide waveguide by fully oxidizing an AlGaAs heterostructure [25], [26].

Because of the heavy mass of Er, its low-energy implantation depth profile is very shallow and unsuitable for providing a gain region in a single-mode waveguide amplifier. In this work, we oxidize AlGaAs doped with Er via multiple high-energy ion implants, and AlGaAs and AlInAs doped during crystal growth by molecular beam epitaxy (Section II-A). The dependence of PL intensity and lifetime of both ion-implanted and *in situ* doped samples are studied for Er concentrations in the range of 0.03–0.27 atomic percent (at.%) in the unoxidized semiconductor. Extensive PL studies are done to optimize the oxidation and annealing process and investigate various quenching mechanisms, including arsenic quenching (Section III-C), hydroxyl quenching (Section IV), and concentration quenching (Section VI). Annealing temperature, time, and As overpressure

Manuscript received April 11, 2002; revised May 17, 2002. This work was supported by National Science Foundation under Grant ECS-9502705 and Grant ECS-0123501.

L. Kou was with University of Notre Dame, Notre Dame, IN 46556 USA. He is now with Compaq, Shrewsbury, MA 40556 USA (e-mail: Leigang.Kou@compaq.com).

D. C. Hall is with Department of Electrical Engineering, University of Notre Dame, Notre Dame, IN 46556 USA (e-mail: dhall@nd.edu).

C. Strohhöfer was with FOM-Institute for Atomic and Molecular Physics, Amsterdam 1098 SJ, The Netherlands. He is now with Fraunhofer Institut für Zuverlässigkeit und Mikrointegration, München D-80686, Germany.

A. Polman is with FOM-Institute for Atomic and Molecular Physics, Amsterdam 1098 SJ, The Netherlands.

T. Zhang was with North Carolina State University, Raleigh, NC 27695 USA. He is now with the Transistor-Capacitor Business Group of Applied Materials, Inc., Santa Clara, CA 95054 USA.

R. M. Kolbas is with Department of Electrical and Computer Engineering, North Carolina State University, Raleigh, NC 27695 USA.

R. D. Heller, Jr., and R. D. Dupuis are with the Microelectronics Research Center at The University of Texas at Austin, Austin, TX 78712 USA.

Digital Object Identifier 10.1109/JSTQE.2002.801689.

1077-260X/02$17.00 © 2002 IEEE

dependencies are discussed in Section III. Fourier transform infrared (FTIR) transmission spectra of oxide films grown in both water vapor (H_2O) and deuterium oxide (D_2O) are used to study the presence and source of hydroxyl (OH) groups in the wet oxides. High-temperature annealing has been employed as an effective post-processing step to activate erbium ions and remove OH groups. We have shown elsewhere that the addition of trace amounts of oxygen to the nitrogen carrier gas enhances the wet oxidation rates and increases the oxide refractive index with lower Al composition AlGaAs alloys [26], [27]. In Section V, we demonstrate that the introduction of 1000 ppm O_2–N_2 results in a significant enhancement of the Er^{3+} PL intensity and lifetime, with lifetime values (~5.0 ms) similar to those achieved in comparably doped Al_2O_3:Er films prepared by other methods [9], [20].

II. Erbium Incorporation and Experimental Methods

A. Material Preparation

The starting materials employed in this paper are $Al_xGa_{1-x}As$ and $Al_xIn_{1-x}As$ films, grown either by molecular beam epitaxy (MBE) and doped with Er *in situ* during crystal growth, or by metal organic chemical vapor deposition (MOCVD) and doped with Er post-growth by multiple ion implantations. Both techniques permit a higher dose to be distributed more uniformly over a greater depth for a lower peak concentration than achieved with the shallow, low-energy implants of [5]. This prevents ion–ion quenching interactions that occur at higher peak concentrations and allows stronger PL signals, enabling measurement of both luminescence intensity and lifetime for a wide range of sample preparation conditions, essential to the process optimization studies and doping method comparisons presented here. The more uniform Er concentration profiles also permit a meaningful study of the dependence of photoluminescence intensity upon Er concentration (i.e., concentration quenching), as presented in Section VI.

The two doping methods presented here are different regarding profile control and concentration limits. By *in situ* doping with Er during crystal growth, the doping profile can be easily tailored as needed, with a doping depth as deep as the thickness of the AlGaAs layer. However, the highest Er concentration is limited by its solubility in the AlGaAs semiconductor, about 5×10^{17} cm^{-3} and 4×10^{19} cm^{-3} for $Al_{0.4}Ga_{0.6}As$ grown at 580 °C and 400 °C, respectively [28]. In contrast, ion implantation can achieve an Er concentration well above the solubility limit because the Er is not distributed in a thermal equilibrium phase with its host. In this situation, the Er may still aggregate and form clusters during the subsequent thermal oxidation process. This shortcoming may be avoidable by implanting the Er ions after oxidation.

1) Er Incorporation in situ During Molecular Beam Epitaxial Growth: Several AlGaAs and AlInAs samples, grown by MBE for a previous study [28], [29] of Er-doped semiconductors at North Carolina State University, Raleigh, were subsequently provided to the University of Notre Dame, IN, for additional oxidation and photoluminescence studies to further explore the suitability of the native oxides as rare earth hosts. The $Al_{0.8}In_{0.2}As$:Er sample used in this work was grown as a mismatched film on a GaAs substrate, originally for doping calibration, and chosen for this study due to its higher Er effusion cell temperature of 900 °C, yielding an Er concentration of ~0.03 at.%. The $Al_{0.8}In_{0.2}As$:Er layer is ~1.4 μm thick and is capped with a 60 Å GaInAs layer. Three $Al_{0.5}Ga_{0.5}As$:Er samples with different Er concentrations have also been studied. For these, the GaAs substrate temperature is about 550 °C, and the erbium cell temperatures are 900 °C, 950 °C, and 1000 °C, respectively, giving uniform erbium concentrations of about 1.27×10^{19} cm^{-3} (0.029 at.%), 3.97×10^{19} cm^{-3} (0.09 at.%), and 1.14×10^{20} cm^{-3} (0.258 at.%), respectively. The $Al_{0.5}Ga_{0.5}As$:Er layers are also ~1.4 μm thick, and are capped with a 60 Å GaAs layer. The Er concentrations versus Er cell temperature for all samples are based upon a calibration study performed with secondary ion mass spectrometry on several $Al_{0.45}Ga_{0.55}As$:Er samples grown at 540 °C [28]. Er incorporation during the MBE growth of GaAs:Er [30] and AlGaAs:Er [28] has been shown to be independent of substrate temperature.

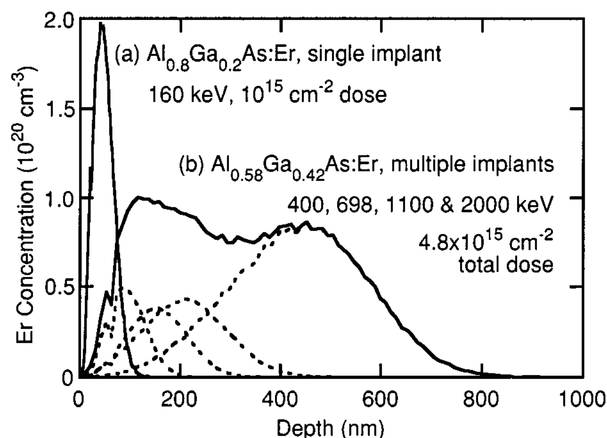

Fig. 1. Erbium concentration doping profiles, simulated by TRIM'98, of (a) $Al_{0.8}Ga_{0.2}As$ doped with 10^{15} cm^{-2} dose by a single low-energy (160 keV) implantation ([5]) and (b) $Al_{0.58}Ga_{0.42}As$ doped with 4.8×10^{15} cm^{-2} dose by four high energy (400, 698, 1100, and 2000 keV) Er^+ implants (this work).

2) AlGaAs With Post-Growth Er Incorporation by High-Energy Ion Implantation: For further studies on oxides of Er-implanted AlGaAs, a 2-μm-thick film of $Al_{0.58}Ga_{0.42}As$ was grown at The University of Texas at Austin by MOCVD, and subsequently doped with Er via high-energy implantation at FOM Institute for Atomic and Molecular Physics (AMOLF), Amsterdam, The Netherlands. The film is grown on a semi-insulating GaAs substrate with a 200-nm GaAs buffer layer, and capped with a 50-nm GaAs cap layer which remains on the sample during implantation. All layers are not intentionally doped. Erbium concentration profiles as simulated by a Monte Carlo analysis with TRIM'98 [31] are shown in Fig. 1. Fig. 1(a) shows for comparison the simulated doping profile of the $Al_{0.8}Ga_{0.2}As$ sample with a single low-energy (160 keV) Er implant (10^{15}-cm^{-2} dose) from our previous study [5]. Except for the discontinuity at the interface between the 20 nm GaAs cap layer and the AlGaAs film, the profile has nearly a Gaussian-shape with a range of 46 nm, a straggle of 18 nm, and a peak Er concentration of about 2×10^{20} cm^{-3} (0.45 at.%). Fig. 1(b) shows the simulated doping profile of the highest dose

(4.8×10^{15} cm^{-2}) multiple high-energy implant sample used in this work. To achieve this relatively flat doping profile to a depth of ~0.5 μm, four implants of singly-ionized Er^{+} are done at 400 keV (4.4×10^{14} cm^{-2}), 698 keV (5.5×10^{14} cm^{-2}), 1100 keV (8.9×10^{14} cm^{-2}), and 2000 keV (2.9×10^{15} cm^{-2}). A flatter profile is possible through further fine-tuning of the implants. For two more lightly-doped samples with total doses of 1.29×10^{15} cm^{-2} and 2.39×10^{15} cm^{-2}, identical implant energies are used but with proportionately lower individual doses. Implantation doses are accurate to ±10%, with the energy stable to within ±2 keV. The implants were carried out at an angle of 7° off normal to avoid channeling, with the sample cooled to 77 K. A Rutherford backscattering spectrometry (RBS) measurement done at AMOLF on the sample with the lowest dose gave a concentration of 0.0675 at.% instead of the 0.05 at.% simulated by TRIM'98. The actual concentration of two other samples, based on the simulated concentration via TRIM'98 and adjusted accordingly, are 0.135 at.% and 0.27 at.% before oxidation. Due to the ~85% shrinkage upon oxidation of AlGaAs, the Er volume concentration (cm^{-3}) in the native oxide is expected to be slightly higher than that in the semiconductor. Most of the As escapes from the crystal during oxidation, while oxygen is incorporated (as most simply illustrated by example of the conversion of 2AlAs to Al_2O_3), so that the number of atoms in a unit volume increases by ~1.25×, reducing the total concentration of Er in atomic percent in the native oxide accordingly. The Er concentrations reported in this paper are given relative to the better-known semiconductor values.

B. Thermal Oxidation and Annealing

Post-implantation anneals typically performed to remove implant damage in crystalline materials were not done in this study. Such anneals are believed to be both unnecessary before the Er-doped semiconductor crystal is oxidized (naturally removing all implantation-induced crystal defects while the material is made amorphous), and undesirable as they would lead to increased precipitation of the Er due to its lower solubility in the semiconductor crystal relative to the oxide. After removing the cap layer, the Al-bearing ternary alloy films described above are thermally oxidized from the surface in a 2-in tube furnace. Oxidations are performed either at 450 °C–500 °C in an atmosphere of water vapor formed by bubbling ultrahigh purity (UHP) N_2 (0.67 L/min) through H_2O at 95 °C (forming a "wet" oxide), or in dry UHP purity O_2 gas at 700 °C–750 °C (without water vapor, forming a "dry" oxide). For wet oxidations with trace amounts of added O_2 (up to 7000 ppm O_2/N_2), a separate, calibrated (5 sccm full scale) mass flow controller channel is used to controllably mix O_2 into the N_2+H_2O process gas stream (Section VI). The water (H_2O) in the bubbler is replaced with 99.8% pure D_2O for some of the wet oxidations to detect the source of OH groups (Section V). Full oxidation is verified by both prism coupler [27] and scanning electron microscopy (SEM) cross-section measurements. In order to activate the Er ions and reduce OH quenching centers (Section III), the wet oxides are annealed open tube in an inert gas ambient (Ar or N_2) at temperatures ranging from 700 °C to 900 °C. A 5–20 min ramp time to the desired annealing temperature prevents oxide delamination problems [32] encountered with rapid thermal processing attempts. We found no observable difference in the PL intensity of Er^{3+} in studies of samples annealed in N_2, Ar, or O_2. Closed-tube annealing in sealed quartz ampoules with varying levels of As overpressure is performed to study the role of As in the native oxide hosts (Section IV).

C. Optical Characterization

Photoluminescence (PL) characterization is performed at room temperature (300 K) by exciting the Er^{3+} with a cw Ti:Sapphire laser tuned to 980 nm, or with either the 488 or 514 nm line of a cw Argon ion laser. Pump powers are typically 500 mW or less, focused to a ~0.5-mm spot size. The pump beam is mechanically chopped at a frequency between 10–20 Hz. The Er^{3+} luminescence is spectrally analyzed using a 0.5 m grating monochromator with a TE-cooled InGaAs detector and lock-in amplifier. Luminescence decay curves are averaged on a digitizing oscilloscope with computer fitting used to extract lifetime values. The cutoff time of the chopper wheel is about 0.22 ms, and the InGaAs detector has a rise time of less than 0.2 ms.

For FTIR transmission spectroscopy measurements, the backside of the samples are mechanically polished to reduce scattering. Because of transmission differences caused by polishing variations, only qualitative comparisons of spectral absorption features are intended.

III. Annealing Process Optimization

A high-temperature annealing process is typically performed with an Er-doped material to favorably modify the host structure and to optically activate the Er ions (through locating them on sites surrounded with more nonbridging O atoms which places them in a trivalently ionized Er^{3+} state), and potentially to suppress PL-quenching nonradiative centers from OH groups and other defects [14], [20], [33]. The results of studies performed to determine the optimal annealing conditions for the Er-doped native oxides in this work are presented here.

A. Annealing Temperature Dependence

Fig. 2 shows the effects of annealing temperature on both PL intensity and the $1/e$ luminescence lifetime, τ, of the Er^{3+} $^4I_{13/2}$ level in native oxides of the implanted $Al_{0.58}Ga_{0.42}As$:Er samples ([Er] $=$ 0.135 at.%). All samples are wet oxidized at a temperature of 500 °C for ~90 min, and then annealed in N_2 for ~10 min at the temperatures shown. The PL peak wavelengths and the spectral full-width at half-maximum (FWHM) remain virtually unchanged upon annealing. The plotted peak PL intensity at 1534 nm increases as the annealing temperature increases, reaching a maximum around 700 °C and then falling off at higher temperatures. Similar behavior was observed in our study of $Al_{0.8}Ga_{0.2}As$ films oxidized following a low-energy Er implant, where at an optimal annealing temperature of ~700 °C, the PL intensity increased by a factor of more than 20 compared to an unannealed oxide [5]. Fig. 2 shows that the lifetimes here remain

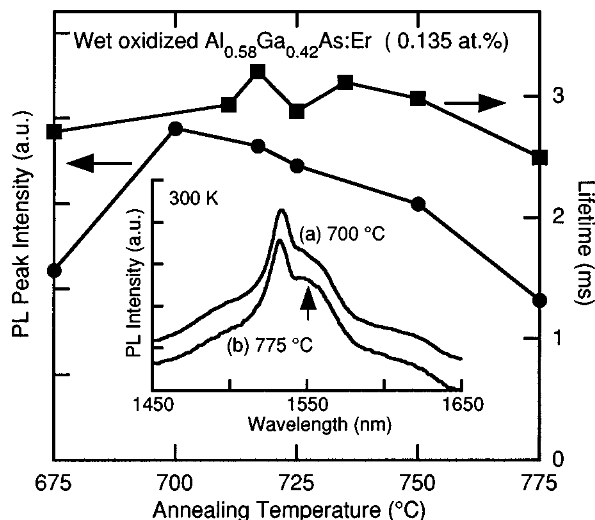

Fig. 2. PL peak intensity at 1.534 μm and the corresponding lifetime measured as functions of annealing temperature for native oxides of $Al_{0.58}Ga_{0.42}As$:Er ($\lambda_{\rm pump} = 980$ nm). All samples are wet oxidized at 500 °C for ~90 min, then annealed in N_2 at the indicated temperature for ~10 min. The inset shows PL spectra of samples annealed at (a) 700 °C and (b) 775 °C, respectively. Spectra (b) was scaled by ~2.1× and shifted along the y axis relative to (a) for comparison. Spectra (a) peaks at 1.534 μm with a 50-nm FWHM.

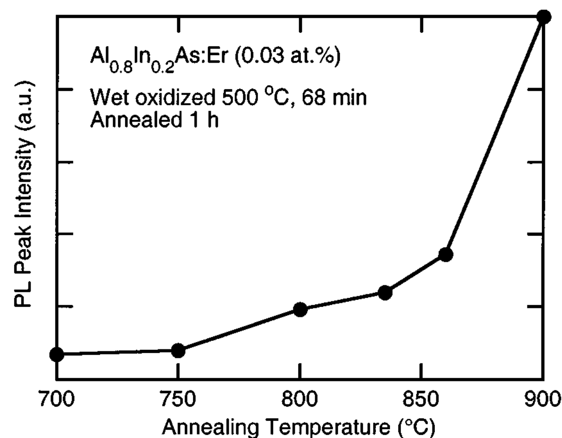

Fig. 3. PL peak intensity at = 1.534 μm measured as a function of annealing temperature for native oxides of $Al_{0.8}In_{0.2}As$:Er ($\lambda_{\rm pump} = 488$ nm). All samples are wet oxidized at 500 °C for about 68 min, and then annealed in Ar atmosphere at the temperature shown for ~1 h.

fairly constant across the entire annealing temperature range, at $\tau = 2.5$–3.2 ms. This suggests that the observed variations in intensity are mainly determined by the fraction of optically active Er^{3+} ions and less by changes in their interactions with quenching mechanisms/centers that alter nonradiative decay rates [9].

In Er-doped Al_2O_3 films fabricated by other techniques [9], [16], [17], the PL intensity is highest for the highest annealing temperature of 950 °C. For Er-implanted Al_2O_3, annealing studies indicate that at temperatures above ~700 °C the primary effect is an increase in the fraction of optically active Er^{3+} ions [9], [14]. Amorphous anodic Al_2O_3 thin films annealed at 800 °C show a phase transition from a gamma-like structure where Al ions are tetrahedrally coordinated in the oxygen lattice to a more alpha-like structure with octahedrally coordinated sites [34]. The larger number of nonbridging O atoms in an octahedral structure will increase the coordination of isolated Er^{3+} ions and reduce Er clustering [1], [17], [22]. We believe that the optimal annealing temperature in this work is reduced compared to other Al_2O_3 hosts by the onset of an "arsenic quenching" mechanism, in which As outdiffusing from the underlying GaAs substrate at higher temperatures is incorporated into the oxide film creating luminescence quenching centers in the form of either defects or optically inactive ErAs precipitates [30]. The inset of Fig. 2 shows PL spectra after annealing at (a) 700 °C and (b) 775 °C. The enhancement of the intensity of the secondary peak centered at ~1545 nm after annealing at 775 °C may indicate a change in the Er ion enviroment, and is seen in other experiments discussed below. The effects of As are explored further in Section III-C.

B. Annealing of AlInAs Oxide

Here, we note the strikingly different annealing behavior that was observed for the oxides of the $Al_{0.8}In_{0.2}As$ film doped with Er during MBE growth. Fig. 3 shows that the PL intensity increases monotonically with annealing temperature until 900 °C, at which point the surface of the oxide film becomes very rough. As the substrate of these samples is GaAs, it is surprising that the arsenic quenching phenomena suggested for AlGaAs:Er oxides has not been observed. Possible explanations include that the presence of In leads to a denser oxide which retards the high-temperature dissociation of the GaAs substrate, or that In somehow suppresses ErAs precipitation or otherwise increases the optical activation of Er in the host. Limited sample availability prevented further study of this unexpected annealing behavior.

C. Arsenic Overpressure Annealing

It is likely that arsenic (As) affects the optical activity of Er dopants in III–V semiconductor oxides. This column V element mostly leaves the crystal upon oxidization, but residual As levels of up to ~2 at.% can remain, primarily coordinated with O in the form of amorphous-As oxides [see [35] and references therein]. The dissociation of the GaAs substrate during high-temperature annealing provides another source of As. It is known that As can combine with Er to form optically inactive ErAs [30]. Wet oxidized AlGaAs films are known to contain significant H content (2 at.% in the native oxide of AlAs), possibly in the form of OH bonded with Al [8]. Arsenic has been shown to reduce levels of OH or H_2O in AlGaAs native oxides annealed in sealed ampoules with As overpressure (~0.1 atm) [36], suggesting it may have a beneficial role here for decreasing luminescence-quenching OH groups. To further investigate the impact of As in the Er-doped native oxide host, we have performed closed-tube annealing with varying levels of arsenic overpressure (As-OP) followed by PL intensity measurements. $Al_{0.58}Ga_{0.42}As$:Er (0.067 at.%) samples oxidized at 500 °C are vacuum sealed in quartz ampoules with a solid As source and annealed at 750 °C for ~20 min. The reference sample (no As-OP) is annealed at 750 °C for ~20 min in N_2 using our standard open-tube technique.

Fig. 4 shows that the PL peak intensity drops quickly with 0.225 atm As-OP, dropping more slowly with increased As-OP

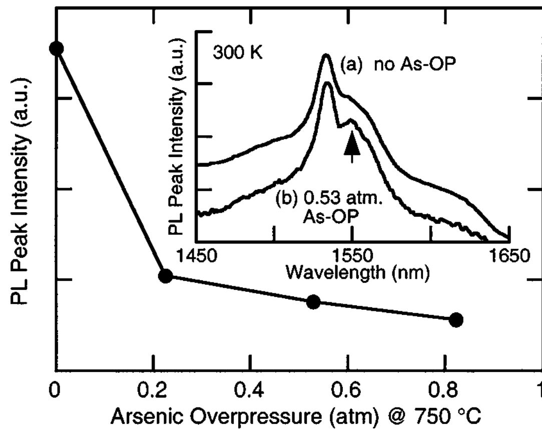

Fig. 4. PL peak intensity of $Al_{0.58}Ga_{0.42}As:Er$ (0.067 at.%) oxidized at 500 °C and then annealed at 750 °C for ~20 min versus variation in arsenic overpressure (λ_{pump} = 980 nm). The inset shows PL spectra of samples (a) annealed open-tube with no As and (b) annealed in a vacuum-sealed quartz ampoule with 0.530 atm As overpressure (As-OP).

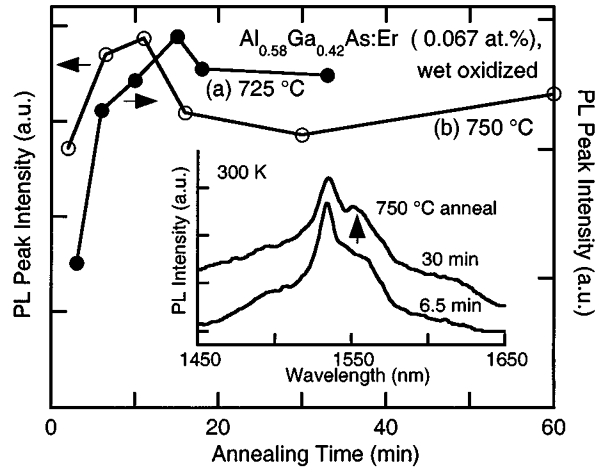

Fig. 5. The dependence of PL peak intensity upon the annealing time of $Al_{0.58}Ga_{0.42}As:Er$ (0.067 at.% Er) wet oxidized at 500 °C for 111 min and then annealed at (a) 725 °C or (b) 750 °C, respectively. The inset is the PL spectra of the samples annealed at 750 °C. Spectra are offset from each other for purposes of comparison.

up to 0.823 atm. As seen in the inset of Fig. 4, the PL spectrum of the sample annealed with 0.53 atm As-OP shows a similar enhancement of the peak around 1547 nm as is observed in Fig. 2(b) for samples annealed open-tube at higher temperatures. It would be useful to study the variations in PL lifetime accompanying the observed intensity changes in Fig. 4 to further elucidate whether they are driven by variations in optical activation levels or nonradiative decay channels [9]. Unfortunately, our limited material availability dictated that these experiments be done with our lowest dose implanted sample that gave insufficient PL signal strength to allow accurate lifetime measurements. The data of Fig. 4 does, however, confirm that increased As levels can negatively impact the luminescence of Er-doped native oxides. Since the As levels incorporated here may not be representative of those occurring during typical sample processing, it is not known whether degradation is the dominant effect. However, a decrease in the fraction of optically active Er ions through the formation of ErAs complexes appears to be the most likely source of the PL intensity decrease for temperatures above 700 °C in Fig. 2 where substrate dissociation occurs more aggressively. Fig. 4 shows that As-OP annealing, typically employed to suppress GaAs substrate dissociation, presents its own problems here, precluding its use for reaching higher the anneal temperatures desirable to most fully activate Er in native oxide films. Performing the Er implantation after oxidation will avoid the interaction of Er and As and formation of ErAs complexes during oxidation when most As is liberated from the crystal, but As outdiffusion from the substrate could still limit the maximum post-implantation annealing temperature.

D. Annealing Time Dependence

Although temperature is the primary factor in the annealing optimization, the anneal time is also subject to optimization. Any desirable solid phase transformation or Er migration that occurs may require a finite time duration, while competing deleterious processes (such as As outdiffusion) place a limit upon the process length. Fig. 5 shows results for $Al_{0.58}Ga_{0.42}As:Er$ samples oxidized at 500 °C for 111 min and then annealed in N_2 at (a) 725 °C or (b) 750 °C for the indicated time durations. The PL intensity increases sharply, reaching a peak at 15 min in (a) and 11 min in (b), and thereafter drops and then stabilizes with increased annealing time. This time dependence suggests that a finite time is required for Er ions to locate on an optically active site, for the native oxide to undergo a favorable microstructure change, and/or quenching-related defects to be eliminated. The optimal annealing time is shorter at higher temperature. These results are consistent with the aggression of a dissociating GaAs substrate causing an increased As content in the native oxide films to worsen any As quenching effect. After an initial decrease in the Er^{3+} PL intensity with increased annealing beyond the optimal time, very little further change occurs. This can be attributed to the rate of As outdiffusion from the oxide reaching an equilibrium with the rate of incorporation of As into the oxide from the GaAs substrate. As mentioned, annealing with As-OP can reduce the OH content of wet oxide films [36]. The slight PL intensity increase going from 30 to 60 min in Fig. 5(b) may be due to a reduction in OH quenching centers, discussed in Section IV.

PL spectra are shown in the inset of Fig. 5 for samples annealed at 750 °C for 6.5 and 30 min. We again note an increase in the intensity of longer wavelength peaks occurring here with longer anneal times. Spectra after a 60-min anneal are very similar to the 30-min spectra (not shown). While a change in relative peak intensities is a manifestation of a change in the relative transition probabilities between the seven Stark-split $Er^4I_{13/2}$ manifold levels and the eight levels of the $^4I_{15/2}$ ground state [1], [2], the cause and significance here is unknown. However, we note a possible correlation in that the effect is observed only for samples annealed here at the highest temperatures (Fig. 2), the highest As overpressures (Fig. 4), and the longest times (Fig. 5). These data suggest that this peak enhancement is correlated to the increased levels of As in the oxide films expected under these annealing conditions. If true, however, it is not necessarily directly due to Er–As interaction, given that similar spectra are observed in As-free Al_2O_3:Er films on

Si [9], [20]. The previously-mentioned As-induced reduction in Al-OH oxide phases may be responsible [36].

IV. Hydroxyl Quenching

The fundamental vibration mode of OH molecules lies between 2500 and 3600 cm^{-1} ($\lambda = 2.7$–$4\ \mu m$), causing the 2nd harmonic of these OH vibrations to overlap with the 1.5-μm emission band of Er^{3+}. Therefore, if an OH^- molecule is coupled to an Er^{3+} ion that is in its first excited state, $^4I_{13/2}$, nonradiative relaxation of the Er^{3+} can occur by excitation of two OH vibrational quanta. Such luminescence quenching by OH groups is well known in various oxide and glass hosts [33]. The wet oxides of Al-bearing III–V semiconductor alloys can be expected to retain hydroxyl groups to some degree due to the inherent nature of wet oxidation. The formation of Al–O–H compounds in AlAs native oxides has been inferred from the significant H content by SIMS analysis [25], [36] and elastic recoil detection (ERD) [8]. Moreover, the wet oxides are known to adsorb moisture from the atmosphere [27] due to their porous microstructure. To further establish the role of OH groups as suspected agents of nonradiative decay, we have previously compared the luminescence properties of $Al_{0.5}Ga_{0.5}As$:Er (0.009 at.%) films oxidized in wet ($N_2 + H_2O$) versus dry (O_2) environments. With the absence of water vapor in the dry oxidation process, the "dry" native oxides provide a similar but OH-free host, resulting in similar spectra but with $\sim$3 times greater PL intensity and a 6.7-ms single-exponential decay lifetime [37]. In this section, we report similar results for wet and dry AlInAs:Er films, discuss FTIR measurements, and a study involving oxidation in deuterium oxide ("heavy water") vapor to investigate the source of OH quenching centers.

A. OH Quenching in Wet Versus Dry AlInAs:Er Oxide Films

In [37], the light Er doping level of the AlGaAs sample resulted in a weak PL signal for the wet oxidized film, preventing measurement of the decay lifetime for comparison to that of the dry oxide. The experiment as repeated with more heavily doped $Al_{0.8}In_{0.2}As$:Er films ($\sim$0.03 at.%) is presented here. Fig. 6 shows PL spectra of $Al_{0.8}In_{0.2}As$:Er and its wet and dry native oxides. Due to a large activation energy for both $Al_{0.5}Ga_{0.5}As$ [37] and $Al_{0.8}In_{0.2}As$ ($\sim$3 eV), dry oxidation is quite slow and must be carried out at a high temperature. The dry oxide of $Al_{0.8}In_{0.2}As$:Er in Fig. 6(a) was formed in O_2 at 725 °C for 135 min, with no post-oxidation anneal. The wet oxide of Fig. 6(b) was prepared through wet oxidation at 500 °C for 81 min, with a post-oxidation anneal in Ar at 725 °C for 1 h. Since the PL intensity from the unoxidized semiconductor has previously been shown to drop after annealing at temperatures higher than 600 °C due to the diffusion and segregation of Er atoms [28], the semiconductor sample of Fig. 6(c) was not annealed. While Fig. 3 shows that higher anneal temperatures can further increase the PL intensity of the AlInAs wet oxide, the anneal temperature is matched here to the 725 °C dry oxidation temperature (chosen to minimize surface roughness) in order to more directly compare OH quenching effects. The data of Fig. 6 are normalized to allow better comparison of spectral features, discussed further below. The PL of the unoxidized

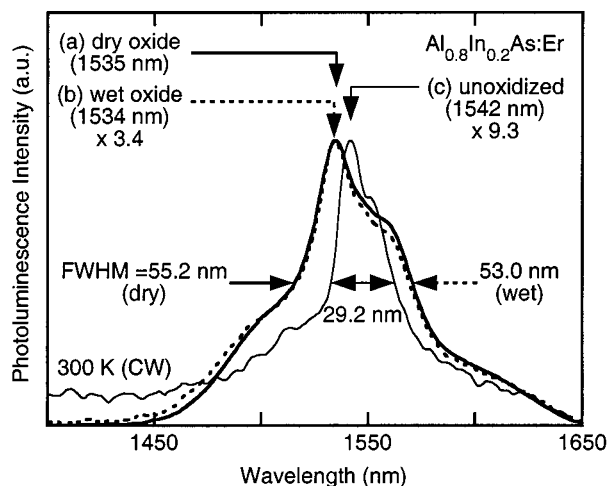

Fig. 6. Room temperature PL spectra from $Al_{0.8}In_{0.2}As$:Er (a) oxidized in pure dry O_2 (725 °C, 135 min), (b) oxidized in water vapor (500 °C, 81 min) and annealed in Ar (725 °C, 1 h), and (c) unoxidized ($\lambda_{pump} = 488$ nm), normalized for comparison. The PL intensity of (a) the dry oxide (peak 1535 nm, 55.2-nm FWHM) is 3.4× stronger than (b) the wet oxide (peak 1434 nm, 53.0-nm FWHM) and 9.3× stronger than (c) the unoxidized semiconductor (peak 1542 nm, 29.2-nm FWHM).

$Al_{0.8}In_{0.2}As$:Er shown in Fig. 6(c) is 9.3 times weaker than that of (a) the dry oxide and 2.7 times weaker than that of (b) the wet oxide. The PL intensity of (a) the dry oxide is 3.4 times greater than that of (b) the wet oxide. The lifetime of the Er^{3+} $^4I_{13/2}$ level is shorter in the wet oxide than in the dry oxide, indicating the presence of more nonradiative decay channels. The dry oxide luminescence has a single-exponential decay with $\tau =$ 5.5 ms, while the wet oxide decay signal is best fit by a double exponential with time constants $\tau_1 \times 1.2$ ms and $\tau_2 \times 6.9$ ms. The fast component is associated with a quenching mechanism causing nonradiative de-excitation of the Er. Similar double exponential behavior with $\tau_1 \times 1.9$ ms and $\tau_2 \times 7$ ms was observed in [5], with the quenching attributed to cooperative upconversion associated with Er–Er interaction in the heavily doped samples. With the lighter doping of these samples, ion–ion interaction is less likely, suggesting another quenching mechanism is at work here (and possibly in [5]). While there are other possible defect-related quenching centers, OH groups are the most probable based on the comparison of wet and dry oxides here. This is supported by FTIR spectra of wet-oxidized AlGaAs films (shown below in Fig. 7) which show a broad OH absorption dip centered at 3410 cm^{-1}, as is also observed in wet oxidized AlAs [38], but which is not present in our unoxidized or dry-oxidized films (data not shown).

Comparing the spectral features in Fig. 6 for both dry and wet oxides, the central peak is at 1.534 and 1.535 μm, respectively, with FWHM of 55 and 53 nm, respectively, indicating a similar local environment for Er^{3+}. We note here that nearly identical spectra are also observed for oxides of AlGaAs:Er doped via ion-implantation (Figs. 2 and 4 insets) or during MBE growth (not shown). All Er-doped oxide spectra are very similar to those of Er-doped deposited Al_2O_3 films [9], [11], [17], [20] and Al_2O_3–GeO_2–SiO_2 glass fibers [39]. The $Al_{0.8}In_{0.2}As$:Er oxide PL spectra is also far broader than the 10-nm FWHM reported for In_2O_3:Er [10]. It is believed that in such multicon-

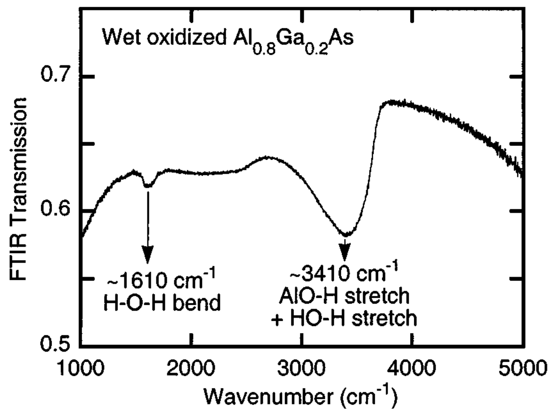

Fig. 7. Normal incidence FTIR transmission spectra of $\sim$1 μm of $Al_{0.8}Ga_{0.2}As$ wet oxidized in H_2O vapor at 500 °C for 25 min. Dip at 3410 cm^{-1} is due to absorption by OH groups and dip around 1610 cm^{-1} is due to the H-O-H bending.

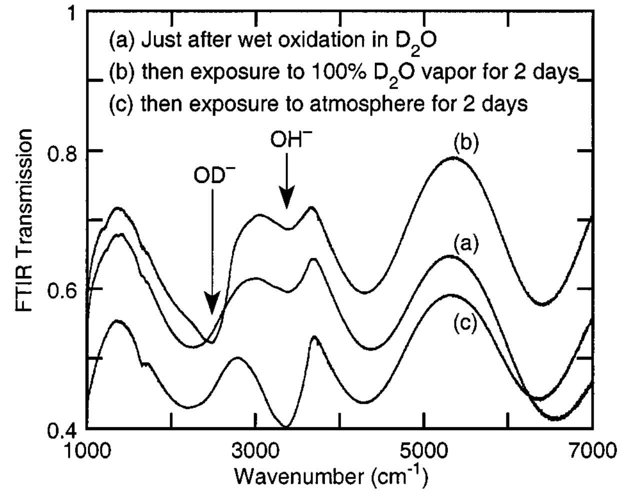

Fig. 8. FTIR spectra of 2-μm $Al_{0.58}Ga_{0.42}As$:Er (0.135 at.%) (a) oxidized at 550 °C for 36 min in D_2O vapor with 4000 ppm O_2 added to the N^2 carrier gas and exposed to atmosphere for only $\sim$20–30 min, (b) and then exposed to 100% relative humidity (RH) D_2O for two days, (c) and then exposed to atmosphere ($\sim$30%–40% RH H_2O) for another two days.

stituent materials that erbium ions preferentially coordinate with the Al-O$^-$ groups which thus have the dominant influence on the crystal field splitting and resulting Er^{3+} Stark levels and transition spectra [39]. In contrast, the inhomogeneous broadening in the crystalline semiconductor host, where each Er ion sees a more consistent crystal field, is much less and results in a FWHM of only 29.2 nm.

B. Infrared Transmission Spectra of AlGaAs Films Oxidized in H_2O Vapor

FTIR transmission spectroscopy has been employed as a sensitive and convenient method to identify OH groups in the oxides, where the absorption band due to the stretching and bending vibrations of the OH-bonded molecules provide a unique spectral signature. Fig. 7 shows the FTIR spectrum of a $\sim$1-μm-thick $Al_{0.8}Ga_{0.2}As$ film [27], wet oxidized at 500 °C for 25 min, which indicates that OH groups in the wet oxides exist in two forms, Al-OH and H-OH. Besides the absorption around 3400 cm^{-1} due to OH stretching, the small dip around 1610 cm^{-1} is due to absorption from H-O-H bending [40]. In general, water absorbs at 3200–3550 cm^{-1} (antisymmetric and symmetric OH stretching) and at 1600–1630 cm^{-1} (H-O-H bending) whereas the hydroxyl complexes of metals lack the H-O-H bending mode near 1600 cm^{-1}.

For liquid water, the ratio of absorption magnitudes at 3410 cm^{-1} to 1610 cm^{-1} is $\sim$1.5:1 [40], indicating that the disproportionate dip in Fig. 7 at 3410 cm^{-1} is due predominately to AlO-H and not HO-H. Thus, most of the OH groups in wet oxides exist in the form of AlO-H, which could be formed either during the wet oxidation process [8] or afterwards through reactions with adsorbed moisture from the atmosphere [27]. The following experiments with D_2O suggest that that later mechanism dominates.

C. Wet Oxidation With D_2O Vapor

Since D_2O has very similar chemical properties to H_2O, the wet oxidation process in D_2O is expected to be similar to that using H_2O. We have explored the wet oxidation of AlGaAs:Er in D_2O vapor to provide further insight into the source of OH groups in the oxides. In order to conserve the D_2O, the oxidations here are carried out at a high temperature ($\sim$550 °C) with the addition of O_2 to further enhance the oxidation rate [26]. We note that oxidation rates in D_2O vapor are $\sim$0.6 times slower than that in normal deionized H_2O vapor. Fig. 8(a) shows the FTIR spectra of an $Al_{0.58}Ga_{0.42}As$:Er ([Er] $=$ 0.135 at.%) film wet oxidized at 550 °C for 36 min in D_2O vapor with 4000 ppm O_2 (relative to N_2) added to the process gas stream. The modulation envelopes evident in all spectra are clearly due to Fabry–Pérot interference effects, as the positions of the maximum and minima shift with the varying thickness of the film layers and incidence angles used in these experiments, while the OH or OD absorption dips remain at a fixed wavenumber. Surprisingly, no absorption due to OD stretching is observed in (a), while the absorption due to OH stretching is still present. The only possible source for OH groups in these films, oxidized in D_2O vapor, is from moisture adsorbed from the atmosphere during the 20–30 min required to transport the sample from the oxidation furnace and mount it in the evacuated FTIR instrument chamber for the measurement.

The FTIR spectra of Fig. 8(b), taken after the sample of Fig. 8(a) is exposed to 100% humidity of D_2O at room temperature for $\sim$2 days, shows a pronounced AlO-D dip around 2500 cm^{-1} while the AlO-H dip becomes shallow. This suggests that OD groups from adsorbed D_2O may incorporate into the oxides, possibly replacing OH groups. As shown in Fig. 8(c), when the same sample is exposed to the ambient room atmosphere again for another two days, the OD-related dips vanish. The FTIR spectra show clearly that the detected OH groups in AlGaAs films oxidized in D_2O vapor with 4000 ppm of O_2 added come predominantly from moisture adsorbed from the atmosphere after oxidation. We did not perform this experiment without the use of added O_2 to isolate its influence in the experiment, but have observed no obvious difference in the strength of OH absorption dips in films oxidized in H_2O with versus without added O_2 (data not shown). These results suggest that with appropriate processing and hermetic

packaging, OH quenching issues in Er-doped wet oxides may be avoidable. We show below in Section V that AlGaAs:Er wet oxidized with added O_2 has PL intensities and lifetimes greater than those of dry oxidized films, suggesting that when prepared in this way, OH quenching is no more of an issue in these materials than in Al_2O_3:Er hosts prepared by other techniques.

It is unclear why in the FTIR spectra of dry oxidized $Al_{0.5}Ga_{0.5}As$ films discussed previously (Section IV-A not shown), no obvious OH absorption bands are detected. Their lower refractive index compared to wet oxides suggest they are more porous, though they are less hygroscopic as indicated by their smaller refractive index increase after exposure to atmospheric moisture. One hypothesis is that the pore surface of the dry oxide is chemically different and less active than in the wet oxide such that adsorbed H_2O will bond only weakly (if at all) with the dry oxides, while reacting and forming chemical bonds with the wet oxides. Thus, when the FTIR chamber is evacuated, the adsorbed moisture inside the dry oxides may evaporate while that in the wet oxides remains. Our FTIR experiments on $Al_{0.5}Ga_{0.5}As$ native oxides annealed at 400 °C, 600 °C, and 700 °C in N_2 suggest that the majority of OH groups detectable in transmission through $\sim$1 μm thick films are removed by 700 °C (data not shown). Some OH groups may still exist, as OH groups in bulk anhydrous aluminum oxides have been found even after heating to 898 °C, disappearing only after heating to 1057 °C [41].

V. Effect of Oxygen Addition to Carrier Gas

The carrier gas used in the wet oxidation process is usually an inert gas, such as N_2 or Ar, and its only function is to transport the reactive agent (H_2O vapor) into the furnace. Thus, it has little effect on the wet oxidation chemical reaction. It has been shown that the wet oxidation process is suppressed with O_2 as the carrier gas [7]. However, we have found for low Al-composition $Al_xGa_{1-x}As$ that adding a trace amount of O_2 $(<1\%)$ to the N_2 carrier gas results in significant increases in oxidation rate $(x \leq 0.8)$ and native oxide refractive index $(x \leq 0.6)$ [26], [27]. In this section, we report the beneficial impact of O_2 addition during wet oxidation upon the luminescent properties of Er^{3+} ions in the oxide.

A group of $Al_{0.58}Ga_{0.42}As$:Er ([Er] $=$ 0.27 at.%) samples were wet oxidized at 450 °C with the addition of varying amounts of O_2 to the process gas, and then annealed at 725 °C for $\sim$12 min in N_2. Fig. 9 shows the dependencies of the Er^{3+} 1.534 μm PL peak intensity and lifetime on the added O_2 amount. The PL intensity increases sharply, about four times, with the addition of only 1000 ppm O_2 (relative to N_2). The PL intensity then drops gradually back toward initial values with further increases in O_2 content up to 7000 ppm. The lifetime of $^4I_{13/2}$ follows a different trend, nearly doubling from 2.6 to 5.0 ms with only 1000 ppm O_2 and remaining above 4 ms until dropping back to to 3.3 ms at 7000 ppm.

Similar results have been observed for $Al_{0.8}In_{0.2}As$ doped with Er during MBE growth (data not shown). The quick saturation of lifetime and refractive index [26] versus the carrier gas oxygen content suggests a different oxide microstructure is formed even with only a small addition of oxygen. A

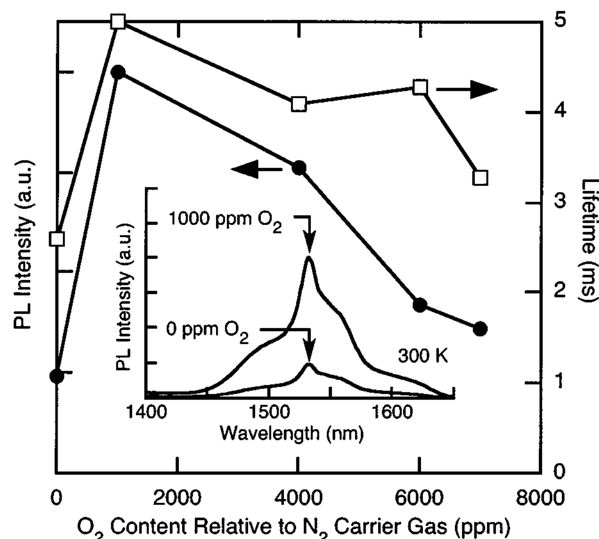

Fig. 9. The dependencies of Er^{3+} 1.534-μm PL peak intensity and fluorescence lifetime on O_2 content in the carrier gas for implanted $Al_{0.58}Ga_{0.42}As$:Er ([Er] = \hbox{0.27} at.%) samples wet oxidized at 450 °C and annealed at 725 °C for $\sim$12 min in N_2. The inset shows the PL spectra and their relative intensities for samples oxidized with no O_2 and with 1000 ppm O_2 added; the later has a 1.533-μm peak and 47-nm FWHM.

more O-rich local environment may serve to suppress some nonradiative transition channels, such as OH or As related quenching centers. However, since the PL intensity increase is more dramatic than the increase in lifetime, it is likely that the O-enriched environment increases the number of nonbridging O atoms which, in turn, effectively coordinate more optically active Er^{3+} ions [39] and prevent Er cluster formation [1], [17], [22].

Rutherford backscattering (RBS) data of $Al_{0.3}Ga_{0.7}As$ wet oxides oxidized with UHP N_2 and with 7000 ppm O_2 content indicate that the ratio of O atoms versus III group elements, (Al $+$ Ga), are 1.35 and 1.51, respectively [26]. This increased ratio is consistent with a more stoichiometric $(Al_xGa_{1-x})_2O_3$ film [8] and confirms that more O atoms are incorporated into the native oxides formed with O_2 added to the process gas.

At the highest O_2 content in Fig. 9, the drop of PL intensity coincides with a drop in oxidation rate, as the added O_2 begins to consume excess hydrogen necessary for the reduction of As_2O_3 (both wet oxidation reaction byproducts) to more volatile elemental As for removal from the oxidizing film [7]. This could result in more Er–As complexes, and thus induce additional As quenching, as discussed in Section III-C.

In Fig. 10, we directly compare the PL decay curves of the Er-implanted $Al_{0.58}Ga_{0.42}As$ (0.27 at.% Er) samples of Fig. 9 oxidized with (a) 1000 ppm O_2 and (c) no added O_2 with the same sample (b) dry oxidized at 725 °C (the same temperature at which (a) and (c) are annealed). The similar lifetimes and single-exponential decay observed for both (a) the O-enriched wet oxide (τ $=$ 5.0 ms) and (b) the dry oxide (τ $=$ 4.6 ms) suggest that O_2 addition during wet oxidation is an effective approach for suppressing the deleterious affects of OH quenching centers discussed above in Section IV, and assumed responsible for the shorter 2.6-ms lifetime of (c), the wet oxide formed w/o added O_2. The $\sim$5-ms lifetimes compare favorably

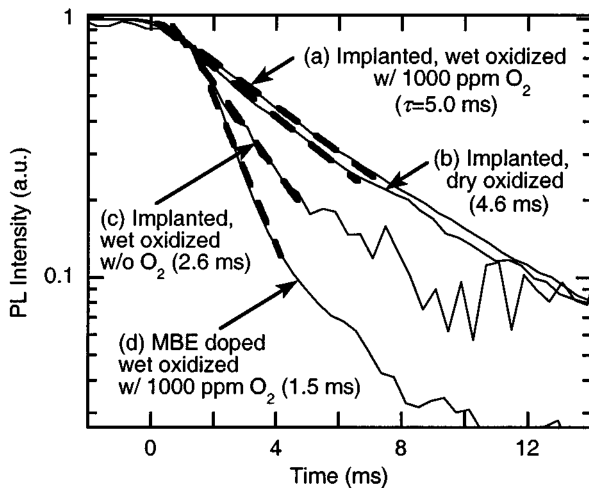

Fig. 10. Room temperature PL decay measurements at 1.534 μm for implanted $Al_{0.58}Ga_{0.42}As$:Er (~0.27 at% Er) (a) wet oxidized at 450 °C with 1000 ppm O_2 added and then annealed at 725 °C in N_2 for 12 min ($\tau = 5.0$ ms) and (b) dry oxidized at 725 °C ($\tau = 4.6$ ms), (c) wet oxidized at 450 °C with no O_2 added and then annealed at 725 °C in N_2 ($\tau = 2.6$ ms), and (d) for $Al_{0.5}Ga_{0.5}As$:Er (~0.26 at% Er) doped during MBE growth, wet oxidized at 500 °C with 1000 ppm O_2 added and annealed at 725 °C in N_2 for 20 min ($\tau = 1.5$ ms).

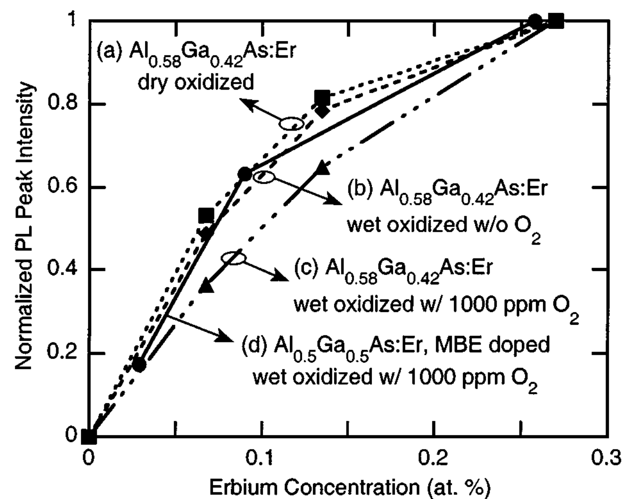

Fig. 11. Normalized PL peak intensity showing concentration quenching characteristics for PL of $Al_{0.58}Ga_{0.42}As$:Er erbium concentration in native oxides with 0.067, 0.135, and 0.27 at.% Er when (a) dry oxidized at 725 °C, or wet oxidized (b) without added O_2 at 501 °C, and (c) with 1000 ppm O_2 added to the N_2 carrier gas at 452 °C; and (d) for $Al_{0.5}Ga_{0.5}As$:Er doped during MBE growth with about 0.029, 0.09, and 0.258 at.% Er, wet oxidized at 500 °C for 132 min with 1000 ppm added O_2. All wet oxides are annealed ~20 min in N_2 at ~725 °C. Sample (c) shows the least concentration quenching, with a 1.54× intensity increase as the Er concentration doubles from 0.235 to 0.27 at.%.

to those reported for Al_2O_3:Er films of comparable doping level [9], [20]. Also shown in Fig. 10(d) is the PL decay curve of $Al_{0.5}Ga_{0.5}As$:Er (~0.26 at% Er) doped during MBE growth and wet oxidized at 500 °C with 1000 ppm O_2 added and annealed at 725 °C in N_2 for 20 min. The MBE-doped sample has a doping level and processing similar to the implanted sample of Fig. 10(a), yet still has a significantly shorter lifetime ($\tau =$ 1.5 ms), indicating a greater density of quenching centers. While there is more uncertainty in the indirectly-inferred doping concentration of sample (c), this comparison points to implantation, a nonequilibrium process unconstrained by the solubility limit of Er in the semiconductor, as a more effective doping technique.

VI. Concentration Quenching

Due to its small emission and absorption cross sections, high concentrations of Er (0.1–1 at.%) are required to realize amplification in a planar waveguide [12], [13], [15]. The maximum Er concentration is constrained by its solubility limit in the host. Increases in gain may not be proportional to the soluble Er concentration as the distances between Er ions become small, resulting in an enhancement of nonradiative de-excitation mechanisms caused by ion–ion interactions [19]. Both energy migration and cooperative upconversion can depopulate the erbium ions in the first excited state and impair the optical gain [14].

We have investigated concentration quenching in samples both doped via ion-implantation and *in situ* during MBE growth. Fig. 11 shows the peak photoluminescence at 1534 nm versus Er concentration for implanted $Al_{0.58}Ga_{0.42}As$ (a) dry oxidized at 725 °C, (b) wet oxidized at 501 °C without added O_2, and (c) wet oxidized at 452 °C with 1000 ppm O_2; and (d) for MBE-doped $Al_{0.5}Ga_{0.5}As$ wet oxidized at 500 °C for 132 min with 1000 ppm O_2. All wet oxides were post-annealed in N_2 at 725 °C for ~20 min. The PL intensities within each group of samples (a)–(d) are normalized by the maximum PL intensity for the purpose of comparing quenching behavior (i.e., the slope, or change in PL signal for change in doping concentration) such that comparisons of relative PL intensity between sample groups from this plot are not valid. The curves are extrapolated to zero as an illustration aid. Concentration quenching is clearly evident in all curves, as the PL intensity does not increase linearly in proportion to increased Er concentration. In the dry oxides of Fig. 11(a), the PL intensity increases only 1.22 times as the Er concentration doubles from 0.135 at.% to 0.27 at.%. Of the three oxidation techniques, samples in (c) prepared by wet oxidation with O_2 added (Section V) exhibit the lowest degree of concentration quenching behavior. For these O-enriched wet oxides of Fig. 11(c), the PL intensity increases 1.54 times as erbium concentration doubles from 0.135 at.% to 0.27 at.%.

The PL intensity is directly proportional to the lifetime and the number of optically active Er atoms [9]. The measured $Er^4I_{13/2}$ level lifetime of the dry oxides of Fig. 11(a) decreases by 0.87× from 5.7 ms at 0.135 at.% to 4.6 ms at 0.27 at.%, with the decrease attributed to the ion–ion interaction between closely spaced ions. However, this lifetime decrease does not account for the entire PL intensity saturation factor as the Er concentration is doubled $(1.22/2.0 = 0.61\times)$, indicating a ~0.7× decrease in the fraction of optically active Er atoms. This is in contrast to the observation with Er-doped Al_2O_3 prepared by sputtering that the fraction of active Er ions does not change with concentrations up to 1 at.% [9].

One possible source of additional nonoptically active sites may be Er clusters formed in either the semiconductor or the oxide during the high temperature oxidation process. Er aggregation most likely happens in the not yet oxidized semiconductor, which has a much lower Er solubility, occurring more aggressively as the Er concentration and/or temperature increases.

This hypothesis is consistent with Fig. 11(a) in which the highest temperature process, dry oxidation, shows the greatest decrease in PL intensity as Er concentration increases. Fig. 11(b) shows that the quenching behavior of $Al_{0.58}Ga_{0.42}As$:Er films wet oxidized at 501 °C without added O_2 is only slightly reduced compared to the dry oxidized films in (a), but significant improvement occurs in (c) where wet oxidation is done with the assistance of 1000 ppm added O_2 at the reduced processed temperature of 452 °C. Both the reduced Er diffusion at the lower temperature and the increased incorporation of O in the oxide films may contribute to a reduction of the rate of apparent Er precipitate formation as doping is increased. The data of Fig. 11(c) suggest that still higher Er concentrations are feasible in these films. Both Er and ErAs precipitate formation [Section III-C] may be dramatically relieved by performing the Er implantation after oxidation. Finally, the pumping efficiency and waveguide amplifier gain in Al_2O_3:Er can be further increased through the use of the codopants such as Yb^{3+} [18], [22], [23] or Eu^{3+} [21].

VII. Conclusion

We have shown that the native oxides of AlGaAs are promising hosts for optically active Er^{3+}, offering the added potential for monolithic integration of planar waveguide amplifiers or lasers with active semiconductor optoelectronic and electronic components. Arsenic liberated from the semiconductor during oxidation or incorporated from the GaAs substrate during high-temperature annealing is shown to be a possible source of quenching centers, most likely through the formation of ErAs precipitates. OH groups in the wet oxides have been detected by FTIR spectroscopy and suggested as probable quenching centers from the comparison of photoluminescence between wet and dry oxides. Oxidation and FTIR experiments employing heavy water (D_2O) suggest that OH groups in AlGaAs wet oxidized with added O_2 come mainly from post-oxidation adsorption of moisture from the atmosphere. The addition of trace amounts of O_2 during wet oxidation is shown to greatly enhance the Er photoluminescence intensity and decay lifetimes. For $Al_{0.58}Ga_{0.42}As$ samples doped via multiple high-energy ion implantation with a peak Er concentration of 0.29 at.%, lifetimes as high as 5.0 ms are achieved.

Acknowledgment

L. Kou would like to thank Dr. S. Raymond for assistance with FTIR measurements.

References

[1] W. J. Miniscalco, "Erbium-doped glasses for fiber amplifiers at 1500 nm," *J. Lightwave Technol.*, vol. 9, pp. 234–250, 1991.
[2] E. Desurvire, *Erbium Doped Fiber Amplifiers: Principles and Applications*. New York: Wiley, 1994.
[3] S. Coffa, A. Polman, and R. N. Schwartz, Eds., "Rare earth doped semiconductors II," in *Proc. Materials Research Society Symp.* , San Fransisco, 1996, vol. 422.
[4] J. M. Zavada, T. Gregorkiewicz, and A. J. Steckl, Eds., "Rare earth doped semiconductors III," in *Mater. Sci. and Eng. B*. Amsterdam, The Netherlands: Elsevier, 2001, vol. 81.
[5] L. Kou, D. C. Hall, and H. Wu, "Room-temperature 1.5 μm photoluminescence of Er^{3+}-doped $Al_xGa_{1-x}As$ native oxides," *Appl. Phys. Lett.*, vol. 72, pp. 3411–3413, 1998.
[6] J. M. Dallesasse, N. Holonyak Jr., A. R. Sugg, T. A. Richard, and N. El-Zein, "Hydrolyzation oxidation of $Al_xGa_{1-x}As$-AlAs-GaAs quantum well heterostructures and superlattices," *Appl. Phys. Lett.*, vol. 57, pp. 2844–2846, 1990.
[7] K. D. Choquette, K. M. Geib, C. I. H. Ashby, R. D. Twesten, O. Blum, H. Q. Hou, D. M. Follstaedt, B. E. Hammons, D. Mathes, and R. Hull, "Advances in selective wet oxidation of AlGaAs alloys," *IEEE J. Select. Topics Quantum Electron.*, vol. 3, pp. 916–926, June 1997.
[8] R. D. Twesten, D. M. Follstaedt, and K. D. Choquette, "Microstructure and interface properties of laterally oxidized $Al_xGa_{1-x}As$," in *Proc. Vertical-Cavity Surface Emitting Lasers, SPIE*, vol. 3003, K. D. Choquette and D. G. Deppe, Eds., 1997, pp. 55–61.
[9] G. N. van den Hoven, E. Snoeks, A. Polman, J. W. M. van Uffelen, Y. S. Oei, and M. K. Smit, "Photoluminescence characterization of Er-implanted Al_2O_3 films," *Appl. Phys. Lett.*, vol. 62, pp. 3065–3067, 1993.
[10] H. K. Kim, C. C. Li, G. Nykolak, and P. C. Becker, "Photoluminescence and electrical properties of erbium-doped indium oxide films prepared by RF sputtering," *J. Appl. Phys.*, vol. 76, pp. 8209–8211, 1994.
[11] R. Serna and C. N. Alfonso, "In situ growth of optically active erbium doped Al_2O_3 thin films by pulsed laser deposition," *Appl. Phys. Lett.*, vol. 69, pp. 1541–1543, 1996.
[12] G. N. van den Hoven, R. J. I. M. Koper, A. Polman, C. van Dam, J. W. M. van Uffelen, and M. K. Smit, "Net optical gain at 1.53 μm in Er-doped Al_2O_3 waveguides on silicon," *Appl. Phys. Lett.*, vol. 68, pp. 1886–1888, 1996.
[13] Y. Yan, A. J. Faber, H. de Waal, P. G. Kik, and A. Polman, "Erbium-doped phosphate glass waveguide on silicon with 4.1 dB/cm gain at 1.535 μm," *Appl. Phys. Lett.*, vol. 71, pp. 2922–2924, 1997.
[14] A. Polman, "Erbium implanted thin film photonic materials," *J. Appl. Phys.*, vol. 82, pp. 1–39, 1997.
[15] M. Benatsou, B. Capoen, M. Bouazaoui, W. Tchana, and J. P. Vilcot, "Preparation and characterization of sol-gel derived Er^{3+}: Al_2O_3-SiO_2 planar waveguides," *Appl. Phys. Lett.*, vol. 71, pp. 428–430, 1997.
[16] S. K. Lazarouk, A. V. Mudryi, and V. E. Borisenko, "Room-temperature formation of erbium-related luminescent centers in anodic alumina," *Appl. Phys. Lett.*, vol. 73, pp. 2272–2274, 1998.
[17] C. E. Chryssou and C. W. Pitt, "Er^{3+}-doped Al_2O_3 thin films by plasma-enhanced chemical vapor deposition (PECVD) exhibiting a 55-nm optical bandwidth," *IEEE J. Quantum Electron.*, vol. 34, pp. 282–285, Feb. 1998.
[18] C. E. Chryssou, C. W. Pitt, P. J. Chandler, and D. E. Hole, "Photoluminescence characterization of Er^{3+}/Yb^{3+} co-implanted alumina (Al_2O_3) thin films and sapphire crystals," in *Inst. Elect. Eng. Proc. Optoelectron.*, vol. 145, 1998, pp. 325–330.
[19] R. Serna, M. J. de Castro, J. A. Chaos, C. N. Afonso, and I. Vickridge, "The role of Er^{3+}-Er^{3+} separation on the luminescence of Er-doped Al_2O_3 films prepared by pulsed laser deposition," *Appl. Phys. Lett.*, vol. 75, pp. 4073–4075, 1999.
[20] S. Musa, H. J. van Weerden, T. H. Yau, and P. V. Lambeck, "Characteristics of Er-doped Al_2O_3 thin films deposited by reactive co-sputtering," *IEEE J. Quantum Electron.*, vol. 36, pp. 1089–1097, Sept. 2000.
[21] C. Strohhöfer, P. G. Kik, and A. Polman, "Selective modification of the Er^{3+} $^4I_{11/2}$ branching ratio by energy transfer to Eu3+," *J. Appl. Phys.*, vol. 88, pp. 4486–4490, 2000.
[22] C. E. Chryssou, F. Di Pasquale, and C. W. Pitt, "Improved gain performance in Yb^{3+}-sensitized Er^{3+}-doped alumina (Al_2O_3) channel optical waveguide amplifiers," *J. Lightwave Technol.*, vol. 19, pp. 345–349, 2001.
[23] C. Strohhöfer and A. Polman, "Relationship between gain and Yb^{3+} concentration in Er^{3+}-Yb^{3+} doped waveguide amplifiers," *J. Appl. Phys.*, vol. 90, pp. 4314–4320, 2001.
[24] M. O. Fischer, M. Reinhardt, and A. Forchel, "Room-temperature operation of GaInAsN-GaAs laser diodes in the 1.5-μm range," *IEEE J. Select. Topics Quantum Electron.*, vol. 7, pp. 149–151, Mar.–Apr. 2001.
[25] Y. Luo, D. C. Hall, L. Kou, L. Steingart, J. H. Jackson, O. Blum, and H. Hou, "Oxidized $Al_xGa_{1-x}As$ heterostructure planar waveguides," *Appl. Phys. Lett.*, vol. 75, pp. 3078–3080, 1999.
[26] Y. Luo, D. C. Hall, O. Blum, H. Q. Hou, R. M. Sieg, and A. A. Allerman, *Non-selective wet oxidation of AlGaAs heterostructure waveguides via controlled addition of oxygen*, Univ. of Notre Dame, Notre Dame, IN, 2001.
[27] D. C. Hall, H. Wu, L. Kou, Y. Luo, R. J. Epstein, O. Blum, and H. Hou, "Refractive index and hygroscopic stability of $Al_xGa_{1-x}As$ native oxides," *Appl. Phys. Lett.*, vol. 75, pp. 1110–1112, 1999.
[28] T. Zhang, "Thin Film Deposition and Optical Characterizations of Erbium Doped III-V Semiconductor Heterostructures Grown by Molecular Beam Epitaxy," Ph.D. dissertation, North Carolina State Univ., Raleigh, NC, 1993.
[29] T. Zhang, J. Sun, N. V. Edwards, D. E. Moxey, R. M. Kolbas, and P. J. Caldwell, "Photoluminescence study of energy transfer processes in erbium doped $Al_xGa_{1-x}As$ grown by MBE," in *Proc. Rare Earth Doped Semiconductors, Materials Research Society Symp. Proc.*, vol. 301, G. S. Pomrenke, P. B. Klein, and D. W. Langer, Eds., 1993, pp. 257–262.

[30] I. Poole, K. E. Singer, A. R. Peaker, and A. C. Wright, "Growth and structural characterization of molecular-beam epitaxial erbium-doped GaAs," *J. Cryst. Growth*, vol. 121, pp. 121–131, 1992.
[31] J. F. Ziegler, J. P. Biersack, and U. Littmark, *The Stopping and Range of Ions in Solids*. New York: Pergamon, 1985.
[32] K. D. Choquette, K. M. Geib, H. C. Chui, B. E. Hammons, H. Q. Hou, T. J. Drummond, and R. Hull, "Selective oxidation of buried AlGaAs versus AlAs layers," *Appl. Phys. Lett.*, vol. 69, pp. 1385–1387, 1996.
[33] Y. Yan, A. J. Faber, and H. de Waal, "Luminescence quenching by OH groups in highly Er-doped phosphate glasses," *J. Non-Cryst. Solids*, vol. 181, pp. 283–290, 1995.
[34] B. G. Frederick, G. Apai, and T. N. Rhodin, "Electronic and vibrational properties of hydroxylated and dehydroxylated thin Al_2O_3 films," *Surf. Sci.*, vol. 244, pp. 67–80, 1991.
[35] S.-K. Cheong, B. A. Bunker, T. Shibata, D. C. Hall, C. B. DeMelo, Y. Luo, G. L. Snider, G. Kramer, and N. El-Zein, "The residual arsenic site in oxidized $Al_xGa_{1-x}As$ $(x = 0.96)$," *Appl. Phys. Lett.*, vol. 78, pp. 2458–2460, 2001.
[36] A. R. Sugg, E. I. Chen, N. Holonyak Jr., K. C. Hsieh, J. E. Baker, and N. Finnegan, "Effects of low-temperature annealing on the native oxide of $Al_xGa_{1-x}As$," *J. Appl. Phys.*, vol. 74, pp. 3880–3885, 1993.
[37] L. Kou, D. C. Hall, J. F. Muth, T. Zhang, and R. M. Kolbas, "Photoluminescence of dry-oxidized Er^{3+}-doped $Al_xGa_{1-x}As$," in *Proc. LEOS'98 11th Annu. Meet.*, 1998, pp. 244–245.
[38] A. Fiore, V. Berger, E. Rosencher, N. Laurent, N. Vodjdani, and F. Nagle, "Birefringence phase matching in selectively oxidized GaAs/AlAs optical waveguides for nonlinear frequency conversion," *J. Nonlinear Opt. Phys. Mat.*, vol. 5, pp. 645–651, 1996.
[39] S. P. Craig-Ryan and B. J. Ainslie, "Glass structure and fabrication techniques," in *Optical Fiber Lasers and Amplifiers*, P. W. France, Ed. Boca Raton, FL: CRC, 1991, pp. 72–74.
[40] B. Smith, *Infrared Spectral Interpretation: A Systematic Approach*. Boca Raton, FL: CRC, 1998, vol. 265.
[41] R. S. Smith, *Oxides and Oxide Films*, J. W. Diggle, and A. K. Vijh, Eds. New York: Marcel Dekker, 1976, vol. 4.

Leigang Kou received the B.S. degree in applied physics from Tsinghua University, Beijing, China, the M.S. degree in optics from Shanghai Institute of Optics and Fine Mechanics, Chinese Academy of Sciences, Shanghai, China, and the M.S. degree in electrical engineering from the University of Notre Dame, Notre Dame, IN, in 1992, 1995, and 1998. He is currently working toward the Ph.D. degree at Notre Dame.

He joined the Alpha Development Group of Compaq (now HP), Shrewsbury, MA, in 2001. His research interests include optical properties of III-V semiconductor native oxides, MOS devices, and digital circuits as used in modern VLSI design.

Douglas C. Hall (S'86–M'91) received the B.S. degree in physics from Miami University, Oxford, OH, and the M.S. and Ph.D. degrees in electrical engineering from the University of Illinois, Urbana-Champaign, in 1985, 1988, and 1991, respectively.

He is currently an Associate Professor with the Department of Electrical Engineering, University of Notre Dame, Notre Dame, IN. From 1991 to 1994, he was with the U.S. Naval Research Laboratory, Washington, DC, where he investigated semiconductor high-power laser amplifiers and erbium-doped fiber sources for fiber optic gyroscopes. He has been with Notre Dame since 1994, and his present compound semiconductor materials and device research is focused on understanding and developing new applications of native oxides for optoelectronic, electronic, and integrated optics devices.

Dr. Hall is a member of the IEEE Lasers and Electro-Optics Society, the American Physical Society, the Optical Society of America, and the American Society for Engineering Education.

Christof Strohhöfer received the M.S. degree in physics from Karlsruhe University, Karlsruhe, Germany, and the Ph.D. degree (for work on optical waveguide materials doped with rare earth ions and silver nanocrystals) from the University of Utrecht, The Netherlands, in 1997 and 2001, respectively.

He is currently with the Fraunhofer Institute für Zuverl ässigkeit und Mikrointegration, Munich, Germany. His research interests include optical methods in bioanalysis.

Albert Polman, photograph and biography not available at the time of publication.

Tong Zhang received the B.S. degree in electrical engineering from the University of Electronics Science and Technology, Chengdu, China, the M.S. degree in materials science and engineering from Virginia Polytechnic Institute and State University, Blacksburg, VA, and the Ph.D. degree in materials science and engineering from North Carolina State University (NCSU), Raleigh, NC, in 1982, 1989, and 1993, respectively. His dissertation research included molecular beam epitaxy of III–V compound semiconductor laser and HEMT structures, quantum well structure characterizations, and Erbium doping in III–V compound semiconductor heterostructures.

Currently, he is a member of Technical Staff and a Technology Manager within the contact metallization product division of Applied Materials, Inc., Santa Clara, CA, previously working in the plasma etch product division upon joining the company in 1997. From 1995 to 1997, he was the Etch Section Head in the Semiconductor Division, Raytheon Company, MA. Prior to Raytheon, he was with Integrated Device Technology, since graduating from NCSU. He has authored over 20 publications and holds three U.S. patents.

Robert M. Kolbas (S'77–M'80–SM'00–F'01) received B.S. degrees in electrical engineering and physics from the University of Illinois at Urbana-Champaign, in 1977 and 1979, respectively.

From 1979 to 1985, he was with Honeywell, Inc. as a Principal Research Scientist and a Senior Research Scientist, where he was responsible for the development of intergrated optoelectronic circuits and the growth of semiconductor thin films. He made numerous contributions to the early development of semiconductor quantum-well heterostructure lasers. He has been a Professor since 1985, and was Head of the Department of Electrical and Computer Engineering at North Carolina State University, Raleigh, from 1995 to 2000. His research interests and contributions include II–V semiconductor heterostructures and quantum wells, optoelectronic integrated circuits, quantum well lasers, strained layer lasers, vertical-cavity lasers, ultra-thin quantum wells, carrier collection in quantum wells, phonon assisted simulated emission, AlGaN–GaN heterostructures, and II–VI semiconductor materials and devices. His present interests include tunable light emitting devices, light emission from nanoparticles, rare earth doped semiconductors, wide bandgap semiconductor materials and photonic devices for chem–bio detection.

Mr. Kolbas is a member Sigma Xi and Tau Beta Pi.

Richard D. Heller, Jr. was born in Taylor, TX, on July 14, 1975. He received the B.S.E.E. (with honors) and M.S.E.E. degrees from the University of Texas, Austin, in 1997 and 1999, respectively. He is currently working toward the Ph.D. degree working on the metalorganic chemical vapor deposition of novel InAlGaP quantum well and InP quantum dot based lasers.

He is a Graduate Research Assistant under the supervision of Prof. R. Dupuis.

Russell D. Dupuis (S'68–SM'84–F'87) received the Ph.D. degree in electrical engineering from the University of Illinois at Urbana–Champaign, IL in 1973.

He worked on GaP LED's at Texas Instruments Incorporated, Dallas, TX, from 1973 to 1975. In 1975, he joined Rockwell International, Anaheim, CA, where he was the first to demonstrate that metalorganic chemical vapor deposition (MOCVD) could be used for the growth of high-quality semiconductor thin films and devices, including demonstrating the first injection laser growth by MOCVD. He joined AT&T Bell Laboratories, Murray Hill, NJ, in 1979, where he extended his work to the growth of InP–InGaAsP by MOCVD. In 1989, he joined the University of Texas at Austin as a Chaired Professor. He is currently studying the growth of III–V compound semiconductor devices by MOCVD, including materials in the InAlGaN–GaN, InAlGaAsP–GaAs, and InAlGaAsP–InP systems. He holds the Judson S. Swearingen Regents Chair in Engineering and is a Professor in the Department of Electrical and Computer Engineering and in the Microelectronics Research Center, The University of Texas at Austin. His technical specialties include semiconductor materials and devices, epitaxial growth by MOCVD, and heterojunction structures in compound semiconductors.

Dr. Dupuis is a member of the National Academy of Engineering and a Fellow of the Optical Society of America.